

ARTIFICIAL HINGED-WING BIRD WITH ACTIVE TORSION AND PARTIALLY LINEAR KINEMATICS

Wolfgang Send¹, Markus Fischer², Kristof Jebens³, Rainer Mugrauer⁴,
Agalya Nagarathinam³, Felix Scharstein¹

c/o ANIPROP GbR, Göttingen, Germany

Key words: Biologically-inspired flight, Experimental facilities and techniques, Active torsion

Abstract

An artificial bird is introduced which was developed using two new features in biologically-inspired flight, active torsion and partially linear kinematics. Active torsion rests on well established theoretical predictions in unsteady aerodynamics. The concept of partially linear kinematics is inspired by zoological observations on flying locusts. When the wings flap upwards, the servomotor for the active torsion turns the outer wing from a positive angle of incidence within a short fraction of the flapping period into a negative angle of incidence. Between the turning points the angle of torsion remains constant. Numerical calculations confirm the expected benefits compared to passive torsion.

1 Introduction

Nature has done an ingenious job of integrating the generation of lift and thrust. Its engine for producing thrust without a single rotating part is the flapping wing. Leonardo da Vinci designed the first human flapper with hinged wings. Many attempts were made in the past to mimic birds' flight with technical constructions, among them the remarkable early work of Lippisch [1] before 1930. Birds, insects and fishes apply the

same basic mechanism. This mechanism is an inherent property of the aerodynamic equations derived from the conservation laws for momentum, mass and energy in fluid mechanics. The coupled bending and torsional motion of a 3D wing reduces to a coupled pitching and plunging motion in 2D.

The physics of this motion has widely been investigated. A recently published paper gives a thorough and comprehensive overview of the history and of progress and challenges in flapping-wing aerodynamics [2]. The discovery of the mechanism dates back to 1924 [3] and was a spin-off during research on airplane flutter. This extremely dangerous phenomenon of high technical importance for aircraft stability physically rests on the same mathematical description as animal propulsion does. It is merely the reverse side of the same coin. The one side is producing thrust with a flapping wing to move forward, the other one is winning energy with oscillating wings from a uniform onset flow. Both modes simply differ in the amplitude ratio of the two constituent degrees of freedom pitching and plunging, bending and torsion respectively. High plunging at small pitching produces thrust, low plunging with high pitching extracts energy. The vicinity of transition from one mode to the other one is a domain of almost complete energy conversion up to 90 % according to basic results in unsteady aerodynamics. Large birds probably are able to fly in this range due to their very low drag. The beneficial use of energy extraction from an airstream with flapping wings was first

¹ANIPROP GbR, Sandersbeek 20, D-37085 Goettingen.

²Festo GmbH & Co. KG, D-73734 Esslingen. ³JNTech GbR, D-71116 Gaertringen. ⁴Effekt-Technik GmbH, D-72667 Schlaitdorf.

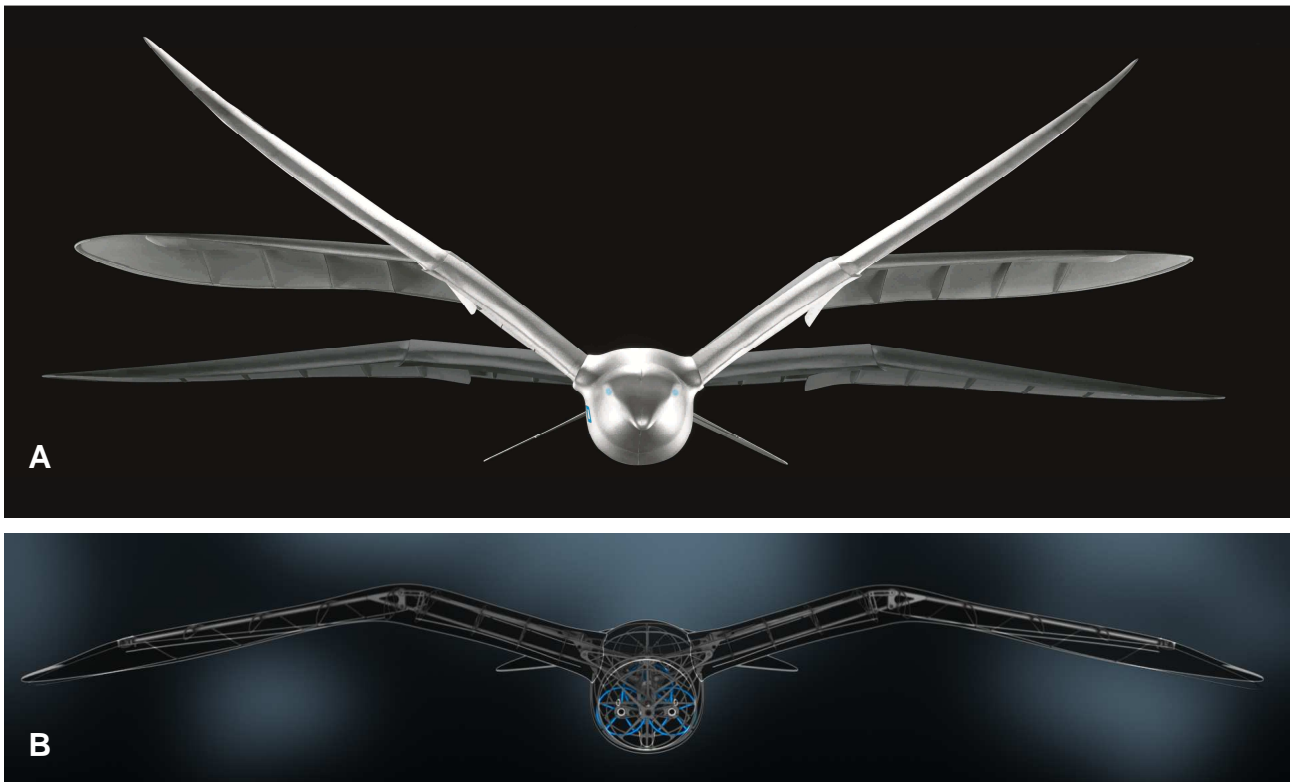


Fig. 1. Front view (A) and X-ray view (B) of *SmartBird*. Span 2 m, planform area 0.5 m², mean chord length 0.25 m, weight 0.48 kg including battery. Operational data at design point: Speed 5 m/s, flapping frequency 2 Hz, average energy consumption 23 W. The model's performance in free flight may be found on the web [14].

investigated in the early 1980s [4] and later extended to the so-called stroke-wing engine for water currents tested in several projects up to 150 kW installed power.

The primary motivation for our research project was a better understanding of the coupled bending and torsional motion and its optimization for potential technical applications. Believing that thrust generation in nature during its long history of evolutionary steps has reached a high level of efficiency we tried to reveal some of its secrets. Our artificial bird serves as technology carrier and demonstrator for encouraging and stimulating research in both directions of producing thrust and using this particular technique for renewable energy resources.

2 The Model

Fig. 1 shows three positions of the articulated wings which are superimposed (A). The X-ray view in the lower part displays the mechanical function (B). The wing consists of a

two-part inner wing spar with an axis suspension at the wing root inside the fuselage, a trapezoidal hinge as is found in a larger format in excavators, and an outer wing spar. Via the trapezoidal hinge, a 1:3 transmission ratio is achieved. The inner wing generates lift, the outer wing across the trapezoidal hinge generates thrust. Both the spars of the inner wing and the outer wing are torsionally stiff. The active torsion is achieved by a servomotor at the end of the outer wing which twists the wing against the spar via the outmost rib of the wing. When *SmartBird* flaps the wing upwards, the servomotor for the active torsion turns the outer wing from a positive angle of incidence within a short fraction of the flapping period into a negative angle of incidence. During these points of turn the angle of torsion remains constant. Through this partially linear motion the flow on the profile is optimally utilized for the generation of thrust. The battery, motor and gear, the crank mechanism and the control and regulating electronics are housed in the fuselage. The external rotor motor flaps the wings up and

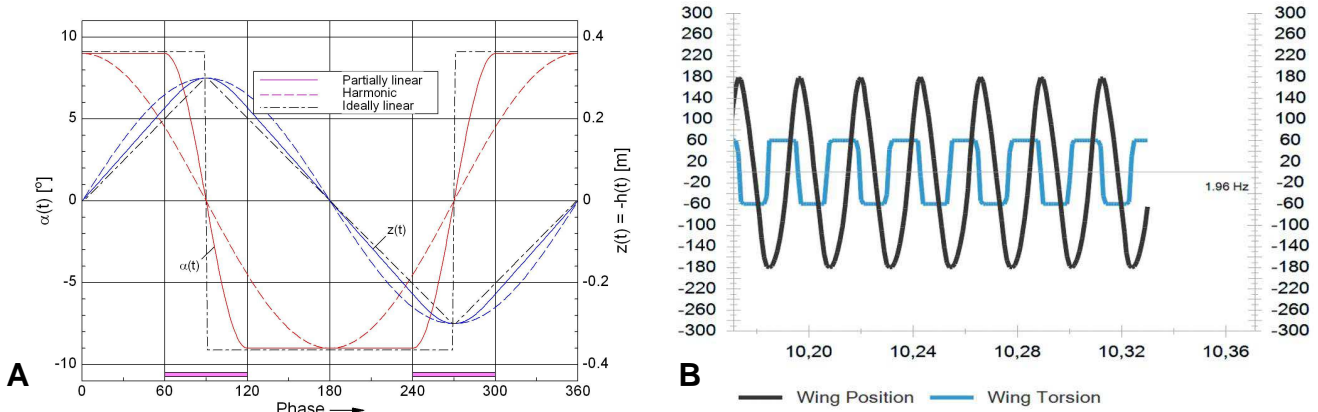


Fig. 2. Kinematics of 2D pitching $\alpha(t)$ and plunging $h(t)$ for partially linear, harmonic and ideally linear motion with typical amplitudes. The torsion shape function for the torsional motion is defined by the amplitude, the beginning and the end of the turn, the slope and the phase shift of the control range (red horizontal bars) versus plunge (A). During operation the motion is continuously monitored. The right part shows a screen shot of the normalized actual torsion shape function during flight relative to the wing tip position (B).

down via a two-stage spur gearing with a 1:45 reduction of speed. The motor is equipped with three Hall sensors to determine the exact wing position. The crank hinge transmits the flapping power from the gear to the outer wing. The crank mechanism does not have a dead center and thus generates a run with low peak loads. This results in smooth flight. The head and the fuselage can be moved synchronously by means of two electric drives and pulleys working in opposite directions. This allows an aerodynam-

ically effective bending of the fuselage and, at the same time, a displacement of weight which makes SmartBird both very agile and flexible. The tail also generates lift. It has both elevator and fin function. When the bird is flying in a straight line, the V-position of the two wings stabilizes the bird, just as a conventional vertical fin stabilizes an airplane. Leading into a curve, the tail is tilted. When the tail tilts on the horizontal axis, the model yaws around the vertical axis. Fig. 2 depicts the basic kinematic relationship and displays a screenshot of the time history of wing tip position and torsion angle. From the aerodynamic point of view these two servomotors and the flapping drive provide the mechanical power which is converted into thrust power. The servomotor which actuates the torsion is controlled using a torsion shape function. Its parameters are interactively accessible during flight.

3 Measurements

The measurements were carried out using an apparatus similar to a carousel (Fig. 3). The technique was developed at the end of the 19th century by E. J. Marey [5], a pioneer in animal flight research. The apparatus named ANIPROP RL3 was recently described [6], however in use since a long time [7]. Different to a normal wind tunnel the model is moved against the air at rest.



Fig. 3. An earlier model flying in the test stand RL3.

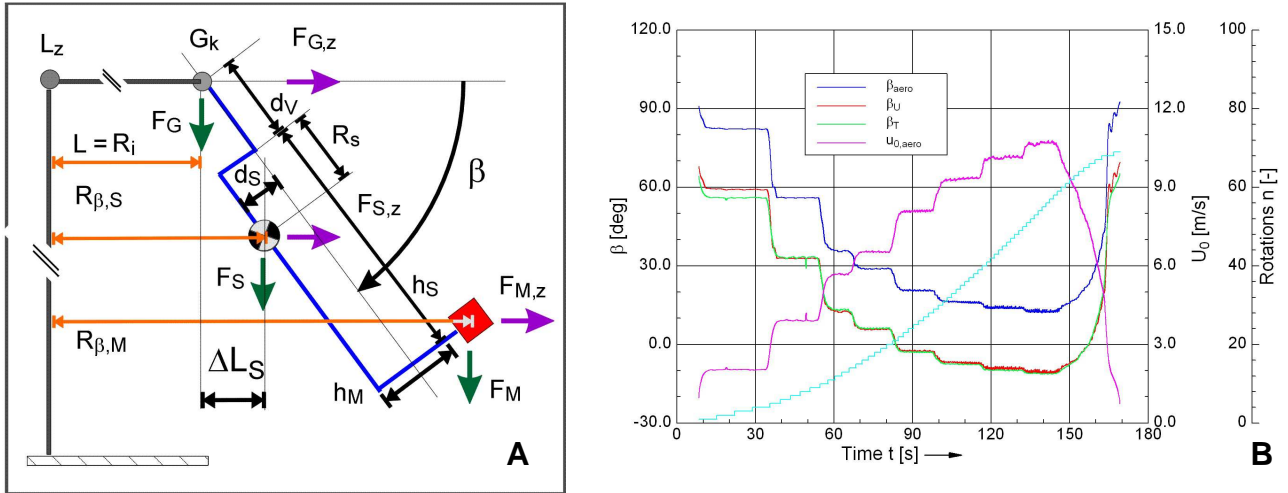


Fig. 4. Side view of the experimental set-up with geometric properties and forces. Gravity force and centrifugal force (index “z”) on inner boom F_G , support F_S and model F_M determine the angle of the outer boom (A). The measured centrifugal angle β_U is expected to coincide with the theoretically determined angle β_T if no lifting model is present (B). The aerodynamic angle β_{aero} must show 90° at rest and 0° for 100 % lift in horizontal flight. $L = 2.17$ m, $d_v + h_s = 1.25$ m. The maximum speed u_0 exceeds 10 m/s. The turquoise step function counts the total number of rotations.

3.1 Experimental Set-up

Fig. 4 shows the side view on the central hub with inner boom and outer boom, which serves as support for the model (red square). The motion is initiated by a towing motor mounted on the central hub. A lever tows the boom and the towing force is recorded using a force sensor of a range ± 50 N. The centre of rotation L_z holds the boom mounted with ball bearings. Nine slip rings transmit operational data and supply the model with electric power instead of a battery in free flight. Angular velocity is measured via the signals coming from a bar-coded disk with 180 bars, which results in 360 position data per rotation. The hinge G_k allows the outer boom to rotate from vertical to horizontal position. The angular sensor inside the hinge determines the centrifugal angle β . The measured angle β_U depends on the weight of the

support, its centre of gravity and its geometric properties.

If the boom is set into motion, the support is deflected by the centrifugal force. Because all quantities including angular velocity are known, the measured angle β_U can also theoretically be predicted. Angle β_T shows the predicted value. Without a lifting model mounted, the measured

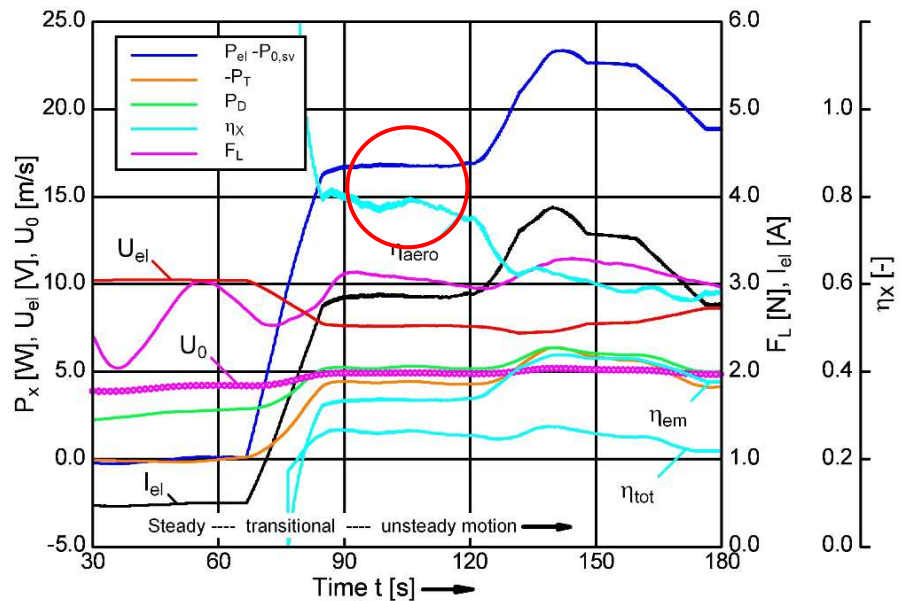


Fig. 5. Aerodynamic efficiency η_{aero} is computed from the measured total efficiency η_{tot} and the previous determination of the electromechanical efficiency η_{em} . $P_{el} - P_{0,sv}$ is the power consumed during the active flight. The almost constant power consumption $P_{0,sv}$ of the control servomotors given by $U_{el} \times I_{el}$ in the steady phase of the measurement amounts to about 5 W. U_0 is the velocity of the model.

angle and the predicted angle are expected to coincide. The difference determines the error which is inherent to subsequent lift measurements. The aerodynamic angle β_{aero} is defined to be 90° at rest. Besides the main contributions to β_T by the quantities mentioned above, a second correction may briefly be mentioned. The inner boom is deflected by its own weight and the weight of the support and the model. We assumed the inner boom to be an elastic beam and determined its stiffness by a static measurement with increasing loads at G_k . The evaluation gives a value for the deflection without external load and can be interpreted as the boom's own weight concentrated in a point load at G_k . Once this point load is known it may be recalculated as uniform line load of the beam. This contribution to β_T amounts to a few degrees. For very low velocities below 2 m/s these assumptions fail to work properly and result in the difference between β_T and β_U which shows Fig. 4 (B). The failure probably is caused by the thin steel cables for the suspension of the boom, when their tension is almost released.

3.2 Results for Tethered Flight

The electrical input power consists of two parts. The servomotors (Fig. 6) consume power even in the case they do no work because they have to hold their position. The power $P_{0,sv}$ is measured and subtracted from the input power. Total efficiency η_{tot} is computed from the ratio of gained thrust power P_T to net input power consumed during active flight:

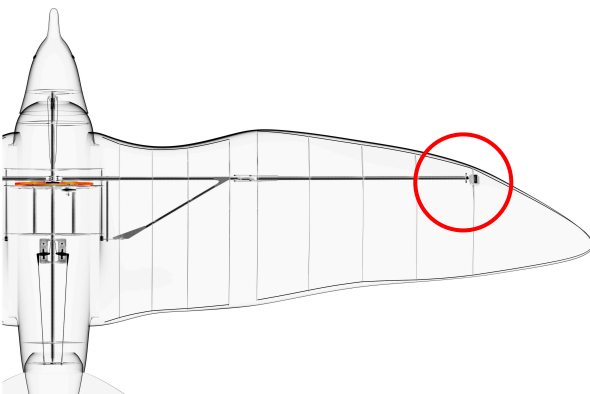


Fig. 6. Position of the torsion servo motor: ○

$$\eta_{tot} = -P_T / (P_{el} - P_{0,sv}) \quad (1)$$

P_T is obtained from the reduction of the towing force F_{tow} during active flight compared to its value F_{SM} in steady motion.

$$P_T = (F_{SM} - F_{tow}) \cdot \frac{R_f}{R_{\beta,M}} \cdot u_0 \quad (2)$$

R_f denotes the lever for the point of origin of the towing force on the boom. Total efficiency η_{tot} is the product of electromechanical efficiency η_{em} and aerodynamic efficiency η_{aero} . We determined the electromechanical efficiency using a dynamometrical brake. The set-up continuously measures torque and angular velocity. For this, the plunging motion of the flapping drive is passed to an axle, which can be loaded by a brake shoe. A force sensor holds the lever of the brake. An angular velocity sensor measures the rotation of the axle. Torque and angular velocity yield the mechanical power.

Electro-mechanical efficiency is the ratio of mechanical power to electrical input power. Aerodynamic efficiency is computed from

$$\eta_{aero} = \eta_{tot} / \eta_{em} \quad (3)$$

Aerodynamic efficiency is the ratio of gained thrust power to mechanical power supplied at all degrees of freedom which contribute to active flight. In our model this is to a vast extent the plunging or bending power. In general, the analysis of animal flight kinematics shows that a third degree of freedom plays an important role which is named the lagging motion. This degree of freedom is not implemented in SmartBird.



Fig. 7. Velocity determined in horizontal free flight.

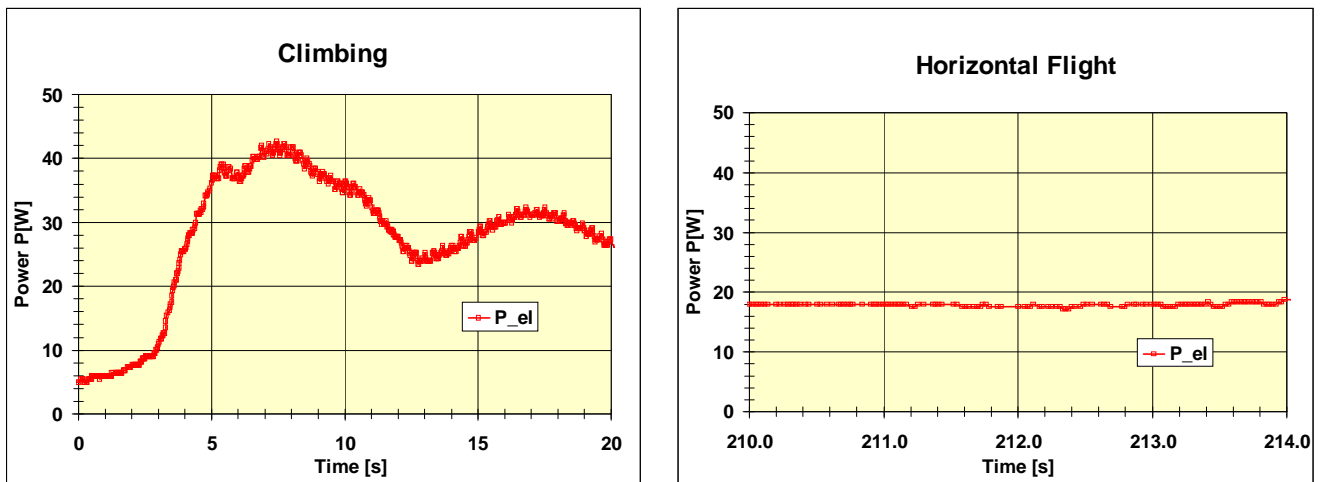


Fig. 8. Total power consumption for free flight during climb and for a typical horizontal flight (18 W).

We were surprised by the high values achieved for η_{aero} above 0.6 and up to 0.8 for an artificial bird which performs remarkably well in free flight. In measurements for earlier models we had obtained values in the same range. However the produced thrust had not been high enough to allow a free flight. The red circle in Fig. 5 marks the domain in which η_{aero} up to 80 % was reached. Measurements in free flight show even lower values for the required electric power than the data during tethered flight. Flight tests show a very sensitive dependence of thrust generation on the torsion shape function.

3.3 On-board Electronics

The on-board electronics allows a precise and thus efficient control of the wing's torsion dependent on its position. Fig. 6 shows the position of the servo motor at the right wing tip. A powerful microcontroller calculates the optimal setting of the two servomotors, which are responsible for controlling the wing torsion. The sequence over time between the flapping and the torsional motion is synchronized by reading the absolute position of the motor for the flapping motion with the aid of the mentioned Hall sensors. The active hinged torsion drive requires a precise coordination of flapping and torsion and thus is continuously monitored. Wing position and wing torsion are monitored by a bi-directional radio communication via ZigBee protocol. It provides operating

data such as battery charge, power input and the control input of the pilot. In addition, the control parameters of the torsion can be set in real time during flight and are optimized and tuned according to the best flight performance. This intelligent monitoring together with the electronic control system makes it possible to adapt the mechanical components to new situations within split seconds. Thus the mechanical construction of the flight model was realized in a simpler, more efficient and weight-optimized manner.

Nevertheless, the precise absolute data of wing torsion and wing bending in free flight as the result of interaction between fluid and structure remain still unknown. Their measurement requires tools which continuously determine the position of the whole flying bird in space. For theoretical calculations the given kinematic input data were applied.

3.4 Results for Free Flight

Determining the velocity in free flight turned out to be difficult without an additional position system. The simple solution for indoor flights was a flight path with a characteristic background. Fig. 7 shows the arrangement with three columns of known distance to each other. The average velocity was determined to be $u_0 = 4.7$ m/s. The consumed power may be related to basic aerodynamic quantities as done in Fig. 5. The net power is obtained from the total power of $P_{\text{el}} = 18$ W by subtracting the bias power of

the servo motors, which is measured during passive flight and amounts to $P_{0,sv} = 5$ W. The net power of $P_{el} - P_{0,sv} = 13$ W has to be multiplied by the measured total efficiency $\eta_{tot} \cong 0.25$ (Fig. 5) in tethered flight and results in a thrust force $F_T = \eta_{tot}(P_{el} - P_{0,sv})/u_0 = 0.7$ N.

The corresponding thrust coefficient reads:

$$c_T = \frac{F_T}{\frac{1}{2} \cdot \rho \cdot u_0^2 \cdot A} = 0.1 \quad (4)$$

A denotes the wing area (0.5 m²), ρ the density of air (1.2 kg/m³). The lift coefficient for a weight of 0.48 kg is given by:

$$c_L = \frac{F_L}{\frac{1}{2} \cdot \rho \cdot u_0^2 \cdot A} = 0.7 \quad (5)$$

These two data lead to the ratio $c_L/c_D \cong 7$ in free sustained horizontal flight. These data are typical of SmartBird. The Reynolds number in horizontal flight amounts to about $Re = 80,000$. The reduced frequency

$$\omega^* = \frac{\omega \cdot c/2}{u_0} \quad (6)$$

ranges from 0.3 to 0.45 . c represents the mean chord length (0.25 m).

4 Theoretical Background

The mechanical construction explained in chapter 2 reflects the theoretical basis [8, 9, 10]. In flapping flight, the amplitude ratio of bending to torsion is the one of two governing parameters at fixed velocity and given flapping frequency. The other one is the phase shift of bending motion versus torsional motion. The typical motion shows the maximum positive torsion angle during upstroke with the turn of the angle at the largest positive elongation of the bending motion, and the highest negative torsion angle during downstroke. As the plunging motion in the original papers [11, 12, 13] begins at the bottom for time equal zero, i.e. the largest negative elongation, and the pitching motion starts with its highest angle of incidence, in flapping flight the phase shift of plunge is defined to be 90° ahead of pitch.

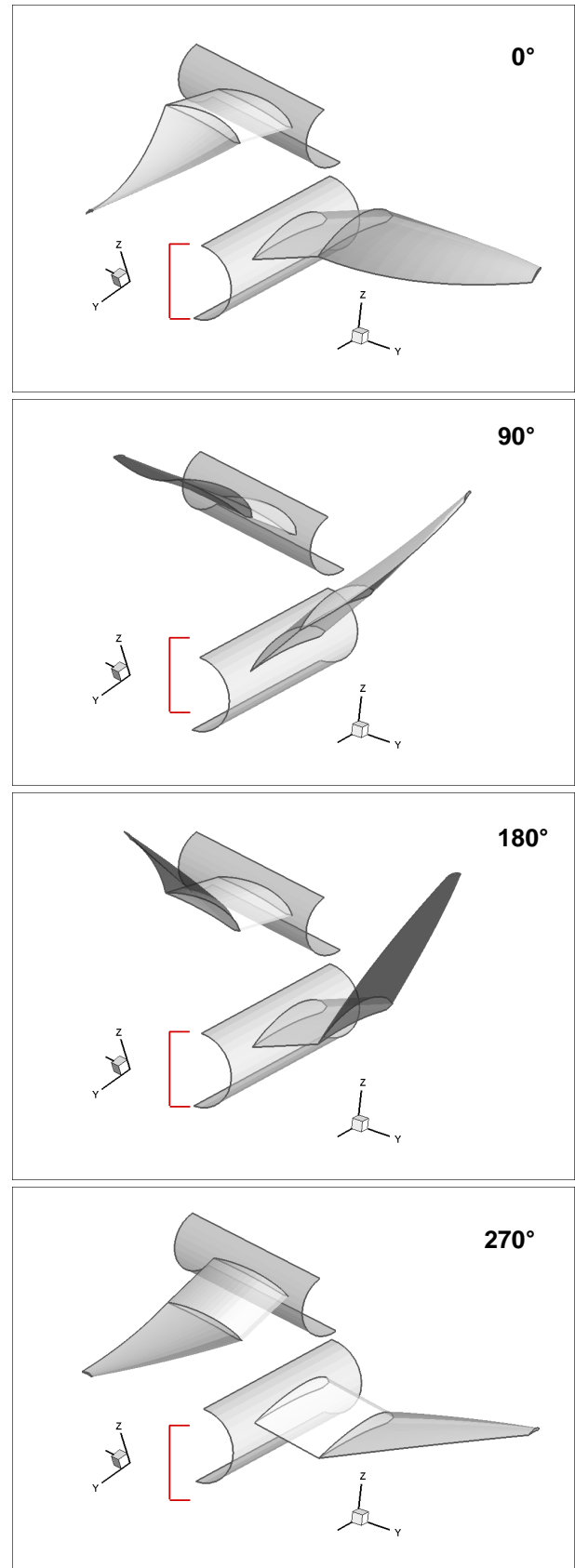


Fig. 9. Kinematics of the articulated wing at four different positions 0° , 90° , 180° and 270° . The motion of the torso is opposite to the wing motion

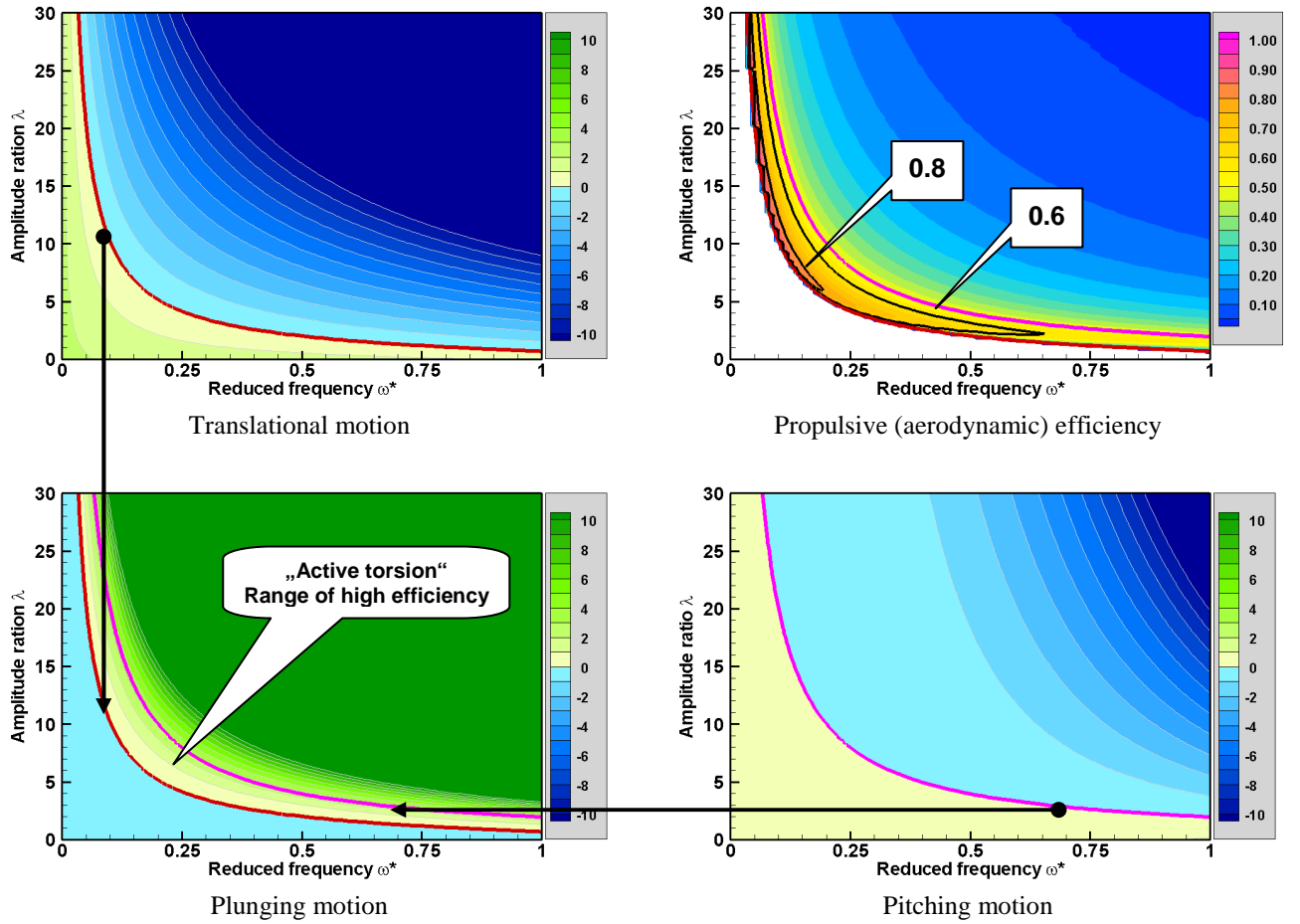


Fig. 10. Mean power coefficients from flate plate theory without the contribution of the so-called “suction force”. Pitch axis set to 0.25 chord length, phase shift $\kappa = 90^\circ$. The propulsive efficiency graph shows contour lines for 0.6 and 0.8 plotted as black solid lines. In blue areas power is gained from the flow, in green areas power is supplied.

The classical theoretical description rests on the assumption of harmonic motion. We introduced a third control feature named the torsion shape function. The torsion shape function turns the harmonic torsion into a partially linear motion. 2D theoretical calculations for the outer wing were made to determine the effect of this type of motion on the aerodynamic efficiency.

4.1 Basic Predictions

Fig. 10 gives an overview of the mechanism of propulsion using the data from thin-plate theory without the contribution of the so-called suction force. This type of thrust theoretically is predicted also for a pure plunging motion. Because the effect originates from the first 3% of a profile’s chord length, it is accompanied by high

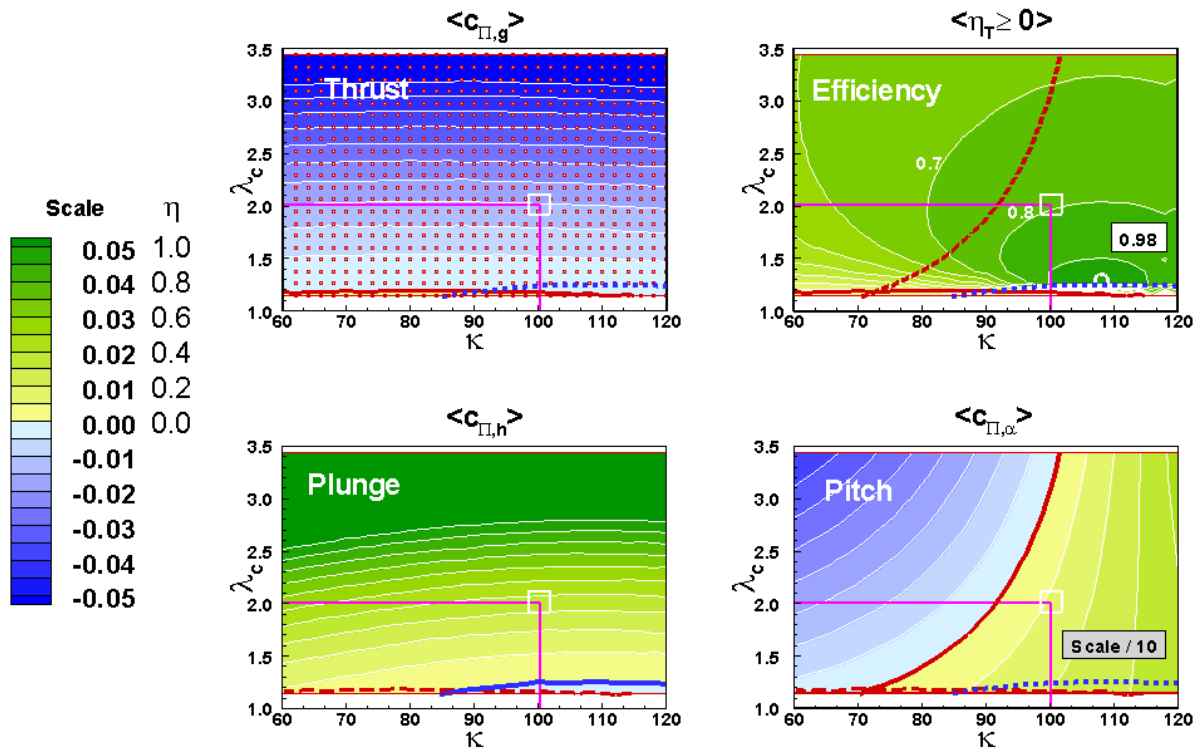
local velocities. Measurements show that the effect tends to disappear for increasing lift. It seems to be that this aspect is a critical issue in theoretical predictions with CFD (Computational Fluid Dynamics).

The amplitude ratio in Fig. 10 is defined as

$$\lambda = \frac{h_0}{\alpha_0 \cdot c/2} \quad (7)$$

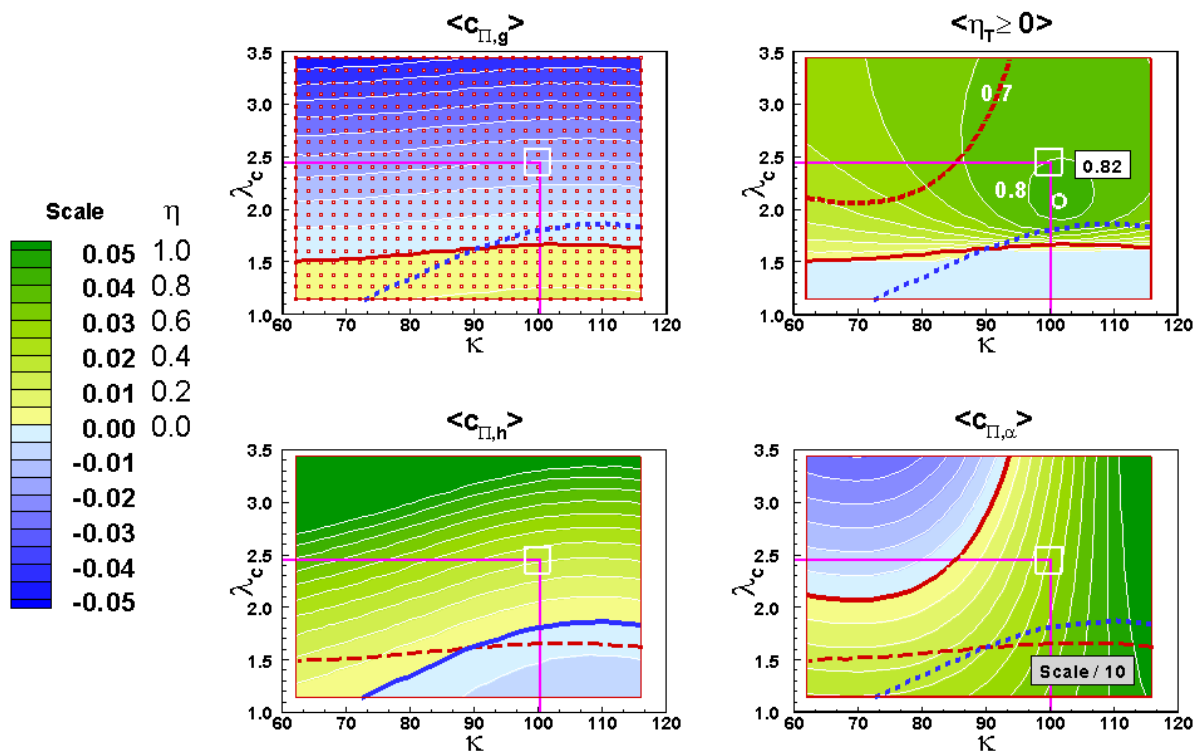
with h_0 and α_0 being plunge and pitch amplitudes. The range of high efficiency is bounded by the requirements of achieving thrust (upper left plot) and working with active torsion (lower right plot). The propulsive or aerodynamic efficiency is the ratio of gained mean thrust power to the sum of supplied power at plunge and pitch.

Each 2D wing section in Fig. 9 is represented by one of these 2D contour plots.



NACA7412 - Mean Power Coefficients and Efficiency - Harmonic Motion

Coupled Plunging and Pitching; $\alpha_0 = 5^\circ$, $\omega_c^* = 0.90$, $\xi_p = 0.4$ - Absolute values



NACA7412 - Mean Power Coefficients and Efficiency - Partially Linear Motion

Coupled Plunging and Pitching; $\alpha_0 = 5^\circ$, $\omega_c^* = 0.90$, $\xi_p = 0.4$ - Absolute values

Fig. 11. Numerical prediction of power coefficients and efficiencies for harmonic and partially linear motion with a 2D Euler code. ξ_p pitch axis, α_0 pitch amplitude. The red squares in the upper left graphs indicate individual solutions.

4.2 Predictions Based on CFD

The basic predictions based on thin plate theory in Fig. 10 can well be compared to the numerical calculations using a CFD tool. Fig. 11 shows the result for harmonic motion and partially linear kinematics. The two figures differ in their definition of amplitude ratio and reduced frequency.

$$\lambda_c = \frac{h_0}{\alpha_0 \cdot c}, \quad \omega_c^* = \frac{\omega \cdot c}{u_0} \quad (8)$$

Data in Fig. 10 are normalized by the square of the pitch amplitude, in Fig. 11 absolute data are displayed. The data refer to the earlier model which is depicted in Fig. 3. The model performed as well as SmartBird except that its wing section was smaller. SmartBird allows for a still lower speed of 4.7 m/s instead of 5 m/s.



Fig. 12. SmartBird's wing section and the section NACA7412 applied during the design process.

The design point ($\eta_{\text{aero}} = 0.8$, $\kappa = 100^\circ$) is selected for a comparison between harmonic and partially linear motion. The amplitude ratio for harmonic motion is much smaller, i.e. the pitch amplitude much higher, than in the case of partially linear kinematics. The fairly wide plateau of high efficiency in Fig. 11 was not found during the flight tests. In summary the observations showed a very sensitive dependence on phase shift and amplitude ratio similar to the narrow range in Fig. 10.

Acknowledgments

The authors gratefully acknowledge the full financial support for the SmartBird project by the Festo company's Bionic Learning Network and his initiator Dr. W. Stoll. We received substantial feedback and were faced with new challenges by the initiator and Dr. H. Frontzek, who played a great role of well grounded advisors.

References

- [1] Lippisch A M. Man Powered Flight in 1929, *Journal of the Royal Aeronautical Society*, Vol. 64 (July 1960), pp 395-398.
- [2] Platzer M F, Jones K D, Joung J, Lai J C S. Flapping-Wing Aerodynamics: Progress and Challenges. *AIAA J.* **46**, pp 2136-2149 (2008).
- [3] Birnbaum W. Das ebene Problem des schlagenden Flügels, *Zeitschrift für angewandte Mathematik und Mechanik (ZAMM)* **4**, pp 277-292, 1924.
- [4] McKinney W, DeLaurier J. The wingmill: An oscillating-wing windmill. *Journal of Energy*, Vol.5, No. 2 (1981), pp 109-115.
- [5] Marey E J. *La Machine Animale*, Paris 1891, Cinquième Édition, Éditeur F. Alcan.
- [6] Send W, Scharstein F., *Thrust Measurement for Flapping-Flight Components*, 27th ICAS Congress, Nice, France, 19-24 September 2010, paper 446.
- [7] Send W, Scharstein F. Artificial Bird in Tethered Flight - Demonstration and Aerodynamics, *Biona Report 13 - Motion Systems*, Gustav Fischer Verlag, Stuttgart 1998, pp 195-196.
- [8] Send W. The Mean Power of Forces and Moments in Unsteady Aerodynamics, *Zeitschrift für angewandte Mathematik und Mechanik (ZAMM)* **72**, pp 113-132, 1992.
- [9] Send W. Flapping-Wing Thrust in Compressible Flow, ICAS 2006-3.10.4, 25th ICAS Congress Hamburg, 3-6 Sep 2006.
- [10] Send W. Der Traum vom Fliegen, *Naturwissenschaftliche Rundschau* **56**, Heft 2, pp 65-73, 2003.
- [11] Küssner H G. Zusammenfassender Bericht über den instationären Auftrieb von Flügeln, *Luftfahrtforschung* **13**, pp 410-424, 1936.
- [12] Theordorsen Th. General Theory of Aerodynamic Instability and the Mechanism of Flutter, N.A.C.A. Report No. 496, 1935.
- [13] Garrick I E. Propulsion of a Flapping and Oscillating Airfoil, N.A.C.A. Report No. 567, 1936.
- [14] Movies showing SmartBird in free flight: http://www.festo.com/cms/en_corp/11369.htm

Copyright Statement

The authors confirm that they, and/or their company or organization, hold copyright on all of the original material included in this paper. The authors also confirm that they have obtained permission, from the copyright holder of any third party material included in this paper, to publish it as part of their paper. The authors confirm that they give permission, or have obtained permission from the copyright holder of this paper, for the publication and distribution of this paper as part of the ICAS2012 proceedings or as individual off-prints from the proceedings.